Chin. Geogra. Sci. 2021 Vol. 31 No. 6 pp. 996−1010
https://doi.org/10.1007/s11769-021-1241-5

Springer Science Press
www.springerlink.com/content/1002-0063

Climate Suitability Assessment of Human Settlements for Regions along the Belt and Road

LIN Yumei[1], LI Peng[1, 2], FENG Zhiming[1, 2], YANG Yanzhao[1, 2], YOU Zhen[1, 2], ZHU Fuxin[3]

(1. *Institute of Geographic Sciences and Natural Resources Research*, *Chinese Academy of Sciences*, *Beijing* 100101, *China*; 2. *College of Resources and Environment*, *University of Chinese Academy of Sciences*, *Beijing* 100049, *China*; 3. *National Tibetan Plateau Data Center*, *Key Laboratory of Tibetan Environmental Changes and Land Surface Processes*, *Institute of Tibetan Plateau Research*, *Chinese Academy of Sciences*, *Beijing* 100101, *China*)

Abstract: Climate is one important environmental variable that affects human life. As the regions along the Belt and Road (B & R) encompass vast territories and large populations, it is significant to assess climate suitability for human settlements, which will influence the migration of various surrounding countries. We selected seven regions including 65 countries along the B & R for the research area and adopted the temperature-humidity index (THI), to assess the climate suitability. We analyzed the spatial characteristics of THI and the correlation between population distribution and THI, the results of which enabled us to adjust the THI classification criteria. We finally assessed the climate suitability of each region. The results reveal that outside the Qinghai-Tibet Plateau, the THI values generally tend to decrease from west to east as longitude increases and downward with increasing latitude. The population distribution is significantly correlated with the THI. Regions with relative suitable climate, including high suitability areas (HASs), moderately suitable areas (MSAs) and low suitability areas (LSAs), account for 50.62% of the total area and encompass in excess of 90% of total population. These areas are widely distributed in the southern regions of 45°N latitude, again with the exception of the Qinghai-Tibet Plateau. Critical suitable area includes 19.48% of the entire area and 8.98% of total population. The non-suitable area accounts for less than 30% of total area, concentrated in the cold high-latitude and high-altitude areas.

Keywords: climate suitability; temperature-humidity index; human settlements; spatial distribution; the Belt and Road

Citation: LIN Yumei, LI Peng, FENG Zhiming, YANG Yanzhao, YOU Zhen, ZHU Fuxin, 2021. Climate Suitability Assessment of Human Settlements for Regions along the Belt and Road. *Chinese Geographical Science*, 31(6): 996−1010. https://doi.org/10.1007/s11769-021-1241-5

1 Introduction

Climate is one important environmental factor that influences human activities and settlements. The influence of climate on human comfort is usually expressed in terms of climate suitability, a biological environmental indicator that is used to evaluate human comfort based on the heat exchange principle between a body and the near-earth atmosphere. A suitable climate facilitates the daily lives of a population and also promotes local socioeconomic development. In contrast, harsh or extreme climates can become restrictive factors hampering activities, interfering with daily production and life, and even adversely influencing health (Hsiang et al.,

Received date: 2021-03-05; accepted date: 2021-08-06

Foundation item: Under the auspices of the Strategic Priority Research Program of Chinese Academy of Sciences (No. XDA20010203, XDA20010201), the Second Tibetan Plateau Scientific Expedition and Research Program (No. 2019QZKK1006), Youth Innovation Promotion Association of the Chinese Academy of Sciences (No. CAS2020055) and National Natural Science Foundation of China (No. 41901086)

Corresponding author: FENG Zhiming. fengzm@igsnrr.ac.cn; ZHU Fuxin. zhufuxin@itpcas.ac.cn

2013; Kjellstrom et al., 2016; Vezzulli et al., 2016; Wu et al., 2016; Matthews et al., 2017). Recently, climate suitability assessment has been the focus of attention in many fields, such as urban planning and design (Kariminia et al., 2016; Yang et al., 2016; Adiguzel et al., 2020), architectural design (Müller et.al, 2014; Rupp et.al, 2015), health risk and healthcare (Błażejczyk et.al, 2018; Napoli et.al, 2018; Aghamohammadi et al., 2021) and tourism (Tang, 2012; Nalau et.al., 2017; Cheng and Zhong, 2019; Amininia et al., 2020; Zhao and Wang, 2021).

One method of assessing climate suitability of human settlements is using biometeorological indices such as the wind effect index (WEI) (Terjung, 1966), the comfort index (CI) (Terjung, 1966), the temperature-humidity index (THI) (Oliver, 1973), physiologically equivalent temperature (PET) (Mayer and Höppe 1987) and universal thermal climate Index (UTCI) (http://www.utci.org). The climate parameters involved in these classic indices include air temperature, relative humidity, wind speed, solar radiation, vapor pressure and mean radiant temperature. However, it is verified that temperature and relative humidity can best predict times when climatic conditions will have a fatal impact on the human body among all the combinations of the adopted climate parameters, as they are both directly related to body heat exchange (Mora et al., 2017). That's why the classic THI is composed of temperature and relative humidity. As THI is applicable to various climatic conditions, including cold, moderate, and hot environments (Emmanuel, 2005), it has been widely adopted to explore the interaction between urbanization and climate change (Emmanuel, 2005; Oleson et al., 2015), the impact of climate change on human health (Vaneckova et al., 2011) and the climate suitability of human settlements (Toy and Kántor, 2017; Kong, 2020; You et al., 2020). In addition, Kong (2020) reports that the climate suitability assessment results based on THI are highly consistent with the results based on the WEI, which implies that THI can perform well in large-scale studies when wind speed and radiation data are lacking.

Climate suitability is a crucial basis in evaluating the livability of human settlements. The results of climate suitability assessment are of great significance for optimizing the spatial distribution of population and construction land, and coordinating the harmonious coexistence of human and nature. Regions along the Belt and Road (B & R) cover vast territories with complex and changeable climate (Han et al., 2018). Most of the areas along the B & R are within developing countries characterized by large rural populations, fragile infrastructures, and poor adaptability. In light of current climate change, all countries will face the same problems such as population mobility and migration and human settlements are likely to experience significant changes. Due to the lack of research and comparative analysis on the climate suitability along the B & R, the aims of this study were therefore to calculate the THI based on climate data at the resolution of 1 km × 1 km, to analyze the relationship between population distribution and the THI, which is the basis for determining the climate suitability zoning standard, and thus to assess the climate suitability of human settlements. The results of this study can provide a basic reference for the construction of human settlements (such as architectural design, urban planning and tourism resource development).

2 Materials and Methods

2.1 Study area

The Belt and Road Initiative (BRI), which aims to promote common development and prosperity of member countries, is a new form of international cooperation that was proposed by China in 2013 (Huang, 2016; Xu, 2018). We selected seven regions including 65 member countries of the BRI as the research objects. Given the total area of each country and their location, we divided these countries into 7 sub-regions (Fig. 1), including China (CN), Southeast Asia (SEA), South Asia (SA), Central Asia (CA), West Asia and the Middle East (WAME), Central and Eastern Europe (CEE), and Mongolia and Russia (MR). These regions span the three continents of Asia, Europe, and Africa, covering a total area of more than 50 million km^2. Regions along the B & R are also home to a large and unevenly distributed population of more than 4.5 billion people, about two-thirds of the global population (Word Bank, 2020). Climate within the B & R zone varies significantly across regions as different regions are diverse including equatorial, dry, warm and humid, cold, and polar climate zones. In the context of global warming, regional climates along the B & R have undergone and will undergo profound changes (Dong et al., 2018; Han et al., 2018), which will significantly alter the livability of different regions, and thus influence regional population migration and flow.

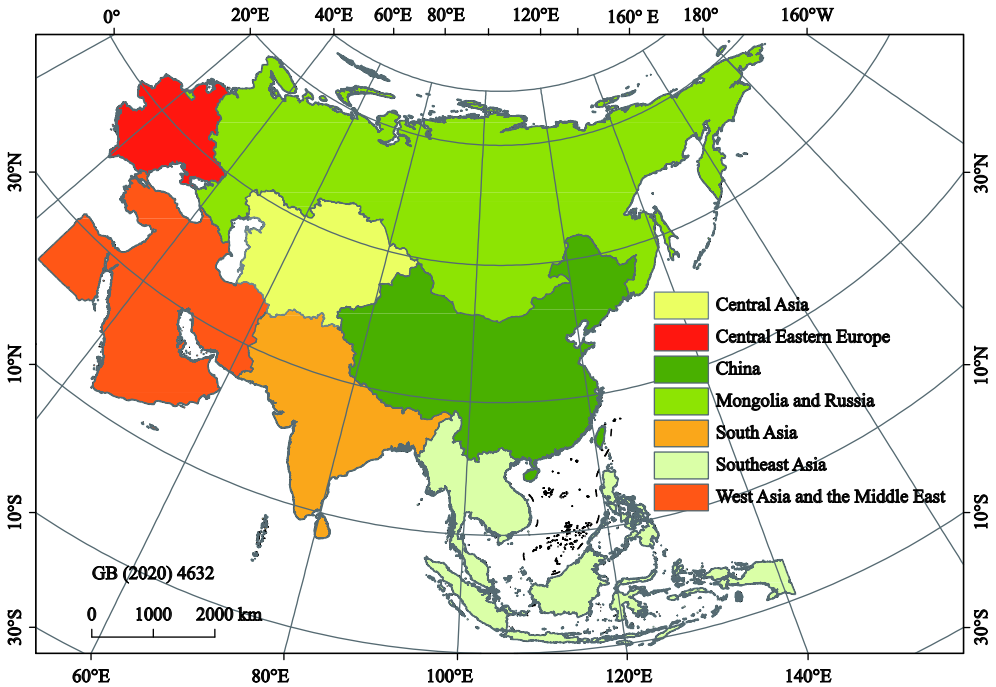

Fig. 1 The selected regions along the Belt and Road

2.2 Data sources and processing

The data used in this analysis mainly include climate and population variables collected at a kilometer grid scale. Climate data mainly include multi-year mean temperature and mean relative humidity, while population data include total population and population density.

2.2.1 Temperature data

The temperature data were derived from the Climatologies at High Resolution for the Earth's Land Surface Areas (CHELSA) dataset (https://chelsa-climate.org/, Karger et al., 2017). This dataset comprises 23 elements collected between 1979 and 2013 at a 30 arc seconds (~1 km) spatial resolution including monthly mean temperature, monthly mean precipitation, annual mean temperature, and mean annual precipitation. Products derived from the CHELSA dataset comprise a geographic coordinate system containing the WGS 84 horizontal datum. This dataset was produced using ERA-Interim-data released by European Centre for Medium-Range Weather Forecast (ECMWF) and it combines global multi-resolution terrain elevation (GMTED2010), atmospheric circulation models, and other multi-source data that has been cross-validated with meteorological station data for different regions over time. We converted the spatial resolution of this compilation from 30″ × 30″ to 1 km × 1 km raster data using the ArcGIS software.

2.2.2 Relative humidity data

As the CHELSA dataset does not contain the relative humidity, the gridded relative humidity was interpolated from in-situ observations. The original relative humidity data used in this study derived from a monthly dataset that comprises 2363 meteorological stations in 65 countries along the B & R provided by the National Meteorological Information Center of China. Daily relative humidity was recorded from each station across the period between 1980 and 2017. We then calculated the multi-year mean relative humidity at each station and utilized the cooperative Kriging method to interpolate the station data. Grid data for annual average relative humidity at a 1 km × 1 km level throughout the area encompassed by the B & R was therefore obtained.

2.2.3 Population data

The total population data for countries along the B & R were derived from the World Bank database. Population density data were adopted from the Land-Scan2015 dataset provided by the Oak Ridge National Laboratory (ORNL) in the United States (https://landscan.ornl.gov/). The dataset is made utilizing an innovative approach based on geographic information system (GIS) data and remote sensing image data. ORNL's LandScan2015 is the community standard for global population distribution. Given a framework of multivariate variance modeling, census information for provincial administrative

units around the world was decomposed into a population distribution database with a resolution of 30 arc seconds. We used GIS technology to obtain the population density dataset at the resolution of 1 km × 1 km of the year of 2015 for countries along the B & R.

2.3 Methods

2.3.1 THI model

In addition to air temperature and relative humidity, other climate data such as wind speed and radiation from weather stations in the B & R areas is not available and the corresponding raster data at the resolution of 1 km is lacking. Given the availability of climate data and the reliability of biometeorological index, we utilized the THI (Oliver, 1973) to evaluate the climate suitability of B & R areas. The physical meaning of the THI is the temperature corrected by the relative humidity, which means that the assessment based on the THI takes into account the comprehensive influence of temperature and relative humidity on human comfort. The THI is calculated as follows:

$$THI = T - 0.55 \times (1 - RH) \times (T - 58) \quad (1)$$

$$T = 1.8t + 32 \quad (2)$$

where T denoted the multi-year mean air temperature in Fahrenheit (°F) collected between 1979 and 2013, while t denoted multi-year mean air temperature in Celsius (°C), and RH is multi-year mean relative air humidity across the period between 1980 and 2017. Due to the limitation of the data availability, the time span of temperature and relative humidity used in this study was inconsistent. Nevertheless, our preliminary calculation shows that the climate states for more than 30 yr are robust for slight time span difference. Therefore, the inconsistent time span of climate factors has very little effect on THI results in the study.

2.3.2 Classification criteria of THI

Studies have reported that people in different regions have different thermal comfort ranges (Hartgill et al., 2011; Pallubinsky et al., 2015; Toy and Kántor, 2017; Pallubinsky et al., 2019). However, THI classification criteria of the existing researches are only applicable to the national scale or sub-regional scale (Tang et al., 2008; Zhong et al., 2019; You et al., 2020). Considering the large research scope of this study, we explored the correlation between population distribution and THI for the regions along the B & R, and then adjusted the existing classification criteria (Tang et al., 2008; Zhong et al., 2019) based on the correlation results, so as to obtain a new set of THI classification criteria applicable to the B & R region.

3 Results

3.1 THI characteristics

Values for the THI were calculated based on processed multi-year mean temperature and relative humidity data for B & R areas. The regional characteristics and spatial distribution of this index was analyzed.

3.1.1 Regional variation

Fig. 2 shows that THI values for regions along the B & R fall between −4 and 80, with large regional differences. Indeed, with the exception of the Qinghai-Tibet Plateau, overall THI values decrease from low to high latitudes.

Results show that 64.28% of regions along the B & R are characterized by THI values between 35 and 75 (Fig. 3). Extremely cold areas with THI values less than 35 account for 29.91% of the whole B & R and are mainly located in the MR region, the northern and southeastern Pamirs within CA, the northeastern China-Tibetan Plateau-Tianshan Mountains zone, and other regions at high latitudes and altitudes. Areas with THI values between 35 and 45 encompass 18.62% of the whole region and are mainly distributed on central-eastern plains within the MR region, in southern Mongolia, in northern CA, in northeastern China, and on the southeastern Qinghai-Tibet Plateau. Areas with THI values between 55 and 75 (i.e., zones where the human body feels relatively comfortable) account for 29.73% of the total area and occur mainly in southern CA, within Egypt in WAME, on the northern Arabian Peninsula, on the Iranian plateau, in western and northern SA, and across most parts of southern China. Regions with THI values greater than 75 tend to have muggy climates and account for 5.81% of the B & R area. These regions are mainly distributed in the southeast of WAME, in coastal areas of southeastern SA, south of the Southeastern Peninsula in SEA, and across most of the Indonesian archipelago.

3.1.2 THI spatial distribution

Trends of THI in longitudinal and latitudinal directions were analyzed across the whole B & R region. Three representative lines of latitude (30°N, 40°N, 50°N) as

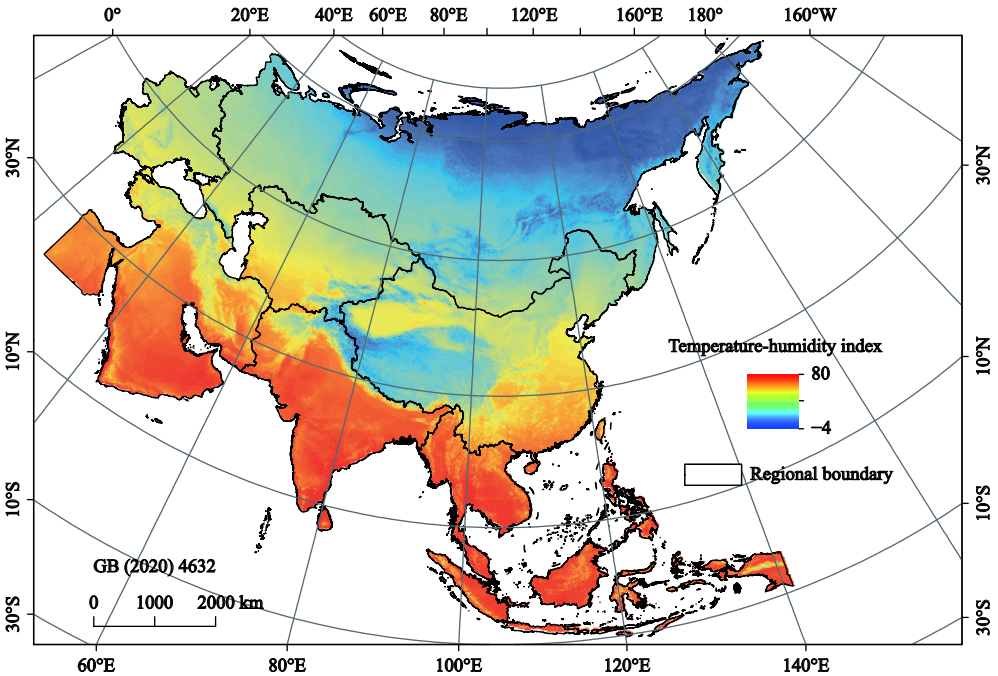

Fig. 2 Regional values for the temperature-humidity index along the Belt and Road

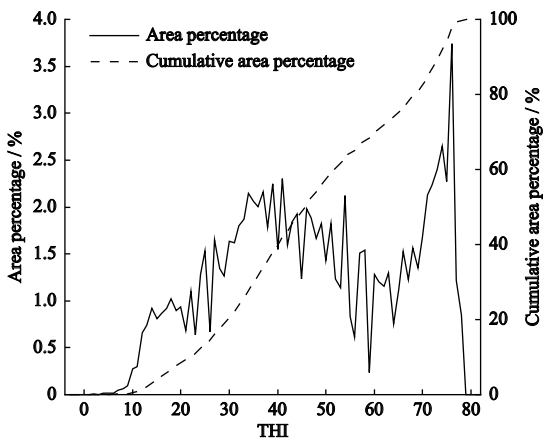

Fig. 3 The variance of area percentage with temperature-humidity index (THI) as well as a cumulative area frequency curve along the Belt and Road

well as three lines of longitude (45°E, 75°E, 100°E) were selected to analyze THI variations.

(1) Changes of THI in latitudinal direction

Fig. 4a reveals variations in mean THI values in a latitudinal direction throughout the B & R. The results show that overall THI tend to decrease from west to east as longitude increases. In a longitude range between 20°E and 75°E, THI remain stable around 50, while between 75°E and 90°E, values gradually drop below 40, mainly due to the presence of the Pamirs and Qinghai-Tibet Plateau at high altitudes and with low mean temperatures. Across a range between 90°E and 120°E, THI rebounds to nearly 50 because of regional terrain reductions. Indeed, to the east of 120°E, THI drop sharply to about 20 because low-latitude regions with high-THI gradually decreases and Russian Far East with high-latitude and low-THI is coming to occupy the dominant position.

Figs. 4b, 4c, and 4d illustrate THI curves at 30°N, 40°N, and 50°N latitudes, respectively. Values of THI at 30°N latitude exhibit spatial distribution characteristics including an east-west high and a middle low with values higher than 60 in most longitude ranges. Values between 75°E and 100°E are significantly lower than 50; the main reason for this remains the presence of the Pamirs and Qinghai-Tibet Plateau characterized by high altitudes and low temperatures. Values of THI in most areas at the 40°N latitude fall within the range between 50 and 60. THI values between 30°E and 40°E and between 70°E and 80°E drop sharply, forming two obvious 'troughs' because the 40°N latitude line passes through the Anatolian Plateau in WAME between 30°E and 40°E and then passes through the Pamirs between 70°E and 80°E where values drop suddenly. The Turan Lowland in CA fall between the two troughs and had THI values as high as 60; when the 40°N latitude line passes through the Tarim Basin from 80°E eastward to 90°E, THI remains stable at a value around 55. Simil-

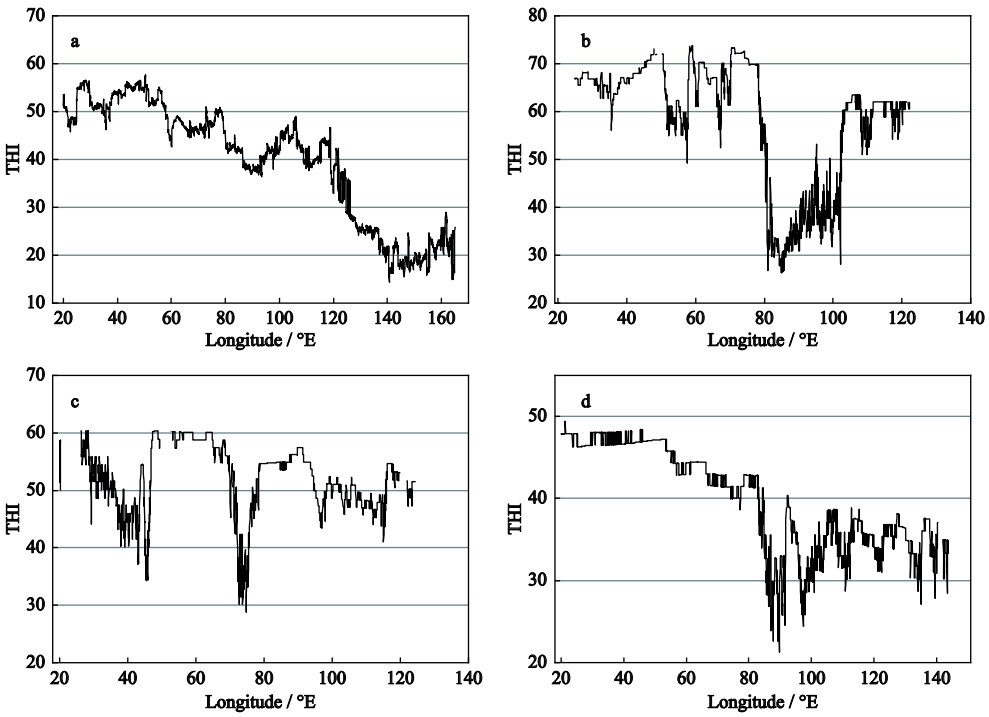

Fig. 4 Changes of temperature-humidity index (THI) in latitudinal direction along the Belt and Road. a indicates latitudinal changes of mean THI. b, c and d indicate latitudinal changes of THI on the lines of 30°N, 40°N and 50°N, respectively

arly, as the 40°N latitude line passes eastward from 90°E through the Loess Plateau and the North China Plain, THI values drop to about 50. While THI in the area west of 80°E on the 50°N latitude line fluctuates just a small amount, remaining between 40 and 50, mainly because these regions are at low altitudes, characterized by flat terrain on the eastern European plains where THI remains relatively high and stable. Values to the east of 80°E fluctuate drastically, because the 50°N latitude line passes through the Kazakh hills, the Mongolian Plateau, and the northern part of the Northeast Plain where terrain undulates.

(2) Changes of THI in longitudinal direction

Fig. 5a reveals change trends of mean THI across B & R regions. Results show that THI values clearly decrease as the latitude increases, consistent with temperature change characteristics.

Figs. 5b, 5c, and 5d reveal longitudinal changes in THI at 45°E, 75°E, and 100°E longitudes. Values of THI along the 45°E longitude line reveal an overall decreasing trend from south to north as latitude increases. Sharp fluctuations in the range between 35°N and 45°N are due to the presence of the Gros Mountains and the Iranian Plateau in WAME where altitude is relatively high and temperature remains relatively low, leading to a sudden THI drop. Values of THI on the 75°E longitude line remain stable at around 70 across the range between 0°N and 32°N. The 'trough' in the range between 32°N and 45°N is mainly due to high-altitude areas across the western Qinghai-Tibet Plateau, the Pamirs, and the Tianshan Mountains. Values of THI along the 100°E longitude line also decreases from low to high latitudes. Due to the presence of the Qinghai-Tibet Plateau, the Badain Jaran Desert, and the Mongolian Plateau between 30°N and 50°N, values of the THI across this region display two troughs and one peak.

Overall, latitude and altitude have more significant impacts on the value of THI compared to longitude. THI values tend to decrease from south to north in the longitudinal direction. On the same latitude line, the THI value of the area with higher altitude is lower than that with lower altitude.

3.2 THI-based climate suitability assessment

Based on the above analysis of THI spatial distribution within regions along the B & R, we revealed the influence of THI on population distribution through analyzing the correlations between the two parameters. The correlation results contributed to the formation of a new of THI classification criteria with reference to the exist-

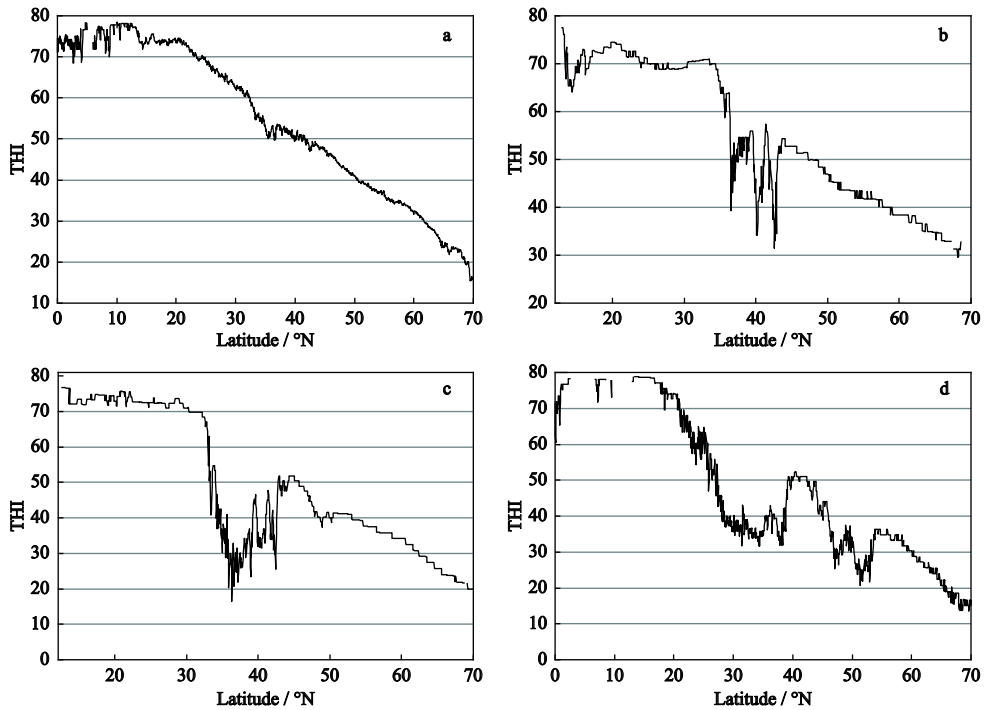

Fig. 5 Changes of temperature-humidity index (THI) in longitudinal direction along the Belt and Road. a indicates longitudinal changes of mean THI. b, c and d indicate longitudinal changes of THI at 45°E, 75°E and 100°E, respectively

ing criteria proposed by previous studies (Tang et al., 2008; Zhong et al., 2019; You et al., 2020). Climate suitability assessment criteria of human settlements was then determined. Finally, a climate suitability assessment based on THI was performed.

3.2.1 Correlations between population density and THI

Correlation analysis results (Fig. 6) show that when THI is higher than 35 and lower than 80, it is significantly correlated with population distribution in regions along the B & R (Pearson's $r = 0.756$, $P < 0.01$), sufficient to show that THI is an important factor influencing population distribution. When THI values are lower than 35, population density is basically zero, which implies that these regions are not suitable for human habitation. But while values fall between 35 and 80, population density tends to fluctuate upwards. Colder regions with THI values between 35 and 45 tend to be sparse populated, comprising less than 4% of the regional population. THI values and the cumulative population distribution curve show that more than 90% of the population in areas along the B & R is concentrated within a range between 45 and 77. Populations in areas with THI values between 60 and 72 account for one-third of the entire B & R region. A set of THI classification criteria (Table 1) applicable to the B & R region is determined combining the correlation results and the existing classification criteria proposed by previous studies (Tang et

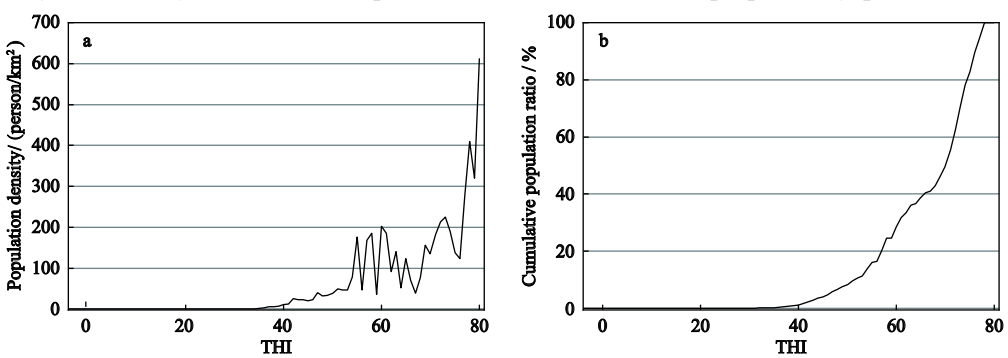

Fig. 6 The curvilinear relationship between population density and temperature-humidity index (a) and a cumulative population density curve (b) along the Belt and Road

Table 1 Classification criteria of temperature-humidity index (THI)

THI	Body perception	THI	Body perception
≤35	Freezing cold	65−72	Snug
35−45	Cold	72−75	Hot
45−55	Slant cold	75−77	Very hot
55−60	Chilly	77−80	Stuffy
60−65	Cool	>80	Extremely stuffy

al., 2008; Zhong et al., 2019; You et al., 2020).

3.2.2 Climate suitability assessment criteria for human settlements

Based on the THI classification criteria (Table 1), regions along the B & R can be divided into non-suitable (NSAs), critically suitable (CSAs), low suitable (LSAs), moderately suitable (MSAs), and high suitable areas (HSAs). Climate suitability assessment criteria for human settlements based on THI are summarized in Table 2.

It is clear that NSAs are regions that are not suitable for human to live for a long time. These regions are extremely cold areas with THI values lower than 35 or extremely sultry areas with THI higher than 80. Similarly, CSAs are regions restricted by climatic conditions that are barely suitable for humans to live all year round. CSAs are areas with THI values between 35 and 45 and between 77 and 80. LSAs are moderately restricted by climatic conditions, generally suitable for human residence all year round. LSAs are areas with THI values between 45 and 55 and between 75 and 77. MSAs are subject to certain climatic conditions, moderately suitable for human life all year round. Climatic conditions in these areas are relatively good, encompassing areas with THI between 55 and 60 and between 72 and 75. HSAs are not subject to climate restrictions, most suitable for humans throughout the year. HSAs have superior climatic conditions with THI values between 60 and 72.

Table 2 Climate suitability assessment criteria for human settlements along the Belt and Road based on temperature-humidity index (THI)

THI	Climate suitability
≤35, >80	Non-suitable areas
35−45, 77−80	Critically suitable areas
45−55, 75−77	Low suitable areas
55−60, 72−75	Moderately suitable areas
60−72	High suitable areas

3.2.3 Climate suitability zoning for human settlements

On this basis of the spatial distribution characteristics of THI as well as climate suitability zoning standards (Table 2), we conducted a climate suitability assessment of human settlements across the whole B & R area. Results (Fig. 7, Table 3) indicate that the overall climate suitability of areas along the B & R shows a band-like distribution pattern, tending to decrease from central to north-south. Regions with suitable climate including HSAs, MSAs, and LSAs account for more than half of the total area and contain in excess of 90% of the total population. The CSAs encompass 19.48% of the total area and carry 8.98% of the total population, while the NSAs account for 29.90% of the total area and 0.18% of the total population. The results indicate that the climate is an important factor affecting regional population distribution.

(1) HSAs

The HSAs within the B & R stretches over 863.17 km^2, 17.23% of the whole area with a population of about 33.99% of the total (Table 3). HSAs are mainly distributed in southern China, the northern Indochina Peninsula in SEA, the southern foothills of the Himalayas in SA, across most parts of WAME, and on the Turan Lowlands in southern CA (Fig.7).

HSAs within WAME are the largest amongst all the seven regions, reaching 394.28 × 10^4 km^2 and encompassing 53.22% of the total area within this region (Fig. 8). This area therefore accounts for 45.68% of total HSAs along the B & R. The corresponding population is 254.89 ×10^6, 59.69% of the total WAME population, which is mainly distributed in Egypt, the Iranian highlands, desert areas of the northern Arabian Peninsula, and the highlands and mountains of the western Arabian Peninsula. Second to WAME, total HSAs within China cover 163.96 × 10^4 km^2, about one-fifth of total B & R area. Corresponding population is 686.03 × 10^6, about half of the total population of the country and more than two-fifths of the total in HSAs along the B & R. The land area of HSAs within the CEE is 0.41 × 10^4 km^2, about 0.19% of regional total area. Similarly, HSAs in CEE encompass 0.66% of the region's population, distributed on the Mediterranean coast of the southwestern Balkan Peninsula Region. No HSA climate zones within the MR are present due to extremely low THI.

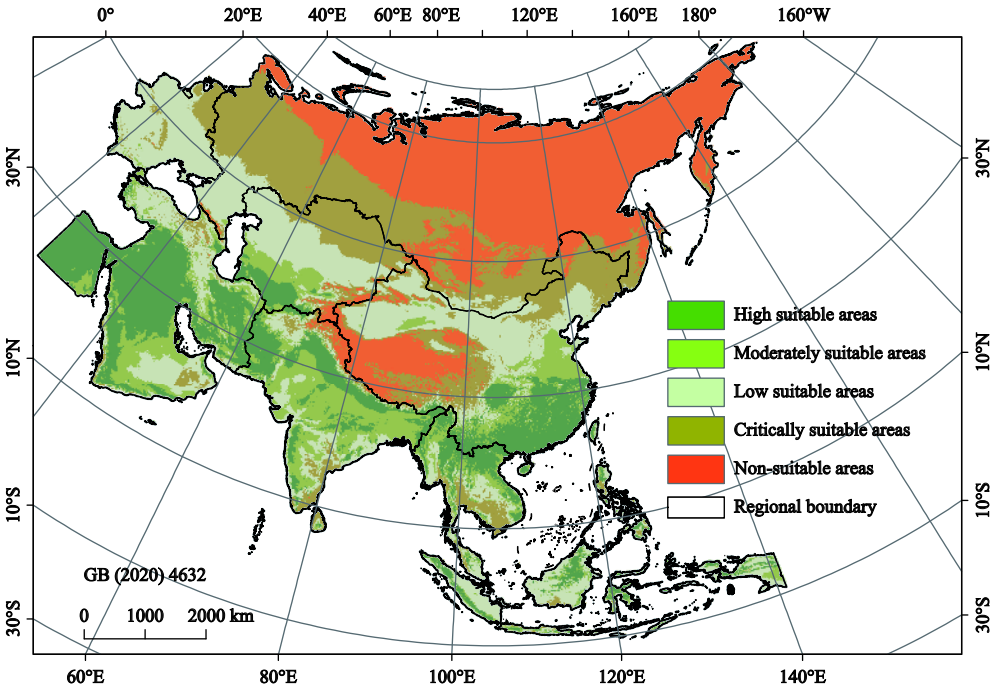

Fig. 7 Climate suitability assessment of human settlements based on the temperature-humidity index in regions along the Belt and Road

Table 3 Area and population of each climate suitability zone along the Belt and Road

Climate suitability zone	HSAs	MSAs	LSAs	CSAs	NSAs
Area /10^4 km^2	863.17	626.19	1046.70	975.86	1498.10
Perception /%	17.23	12.50	20.89	19.48	29.90
Population /10^6	1556.19	1501.82	1101.31	411.25	8.43
Perception /%	33.99	32.80	24.05	8.98	0.18

Note: NSAs means non-suitable areas, CSAs means critically suitable areas, LSAs means low suitable areas, MSAs means moderately suitable areas and HSAs means high suitable areas

HSAs of China and SA are densely populated (Fig. 8), which indicates that the climate suitability matches the population distribution well in this two regions. Although the HSAs of WAME is relatively large, the population density is relatively low compared to China and SA, which implies that in addition to climatic factors, other factors (such as land cover) also have great impact on the human life.

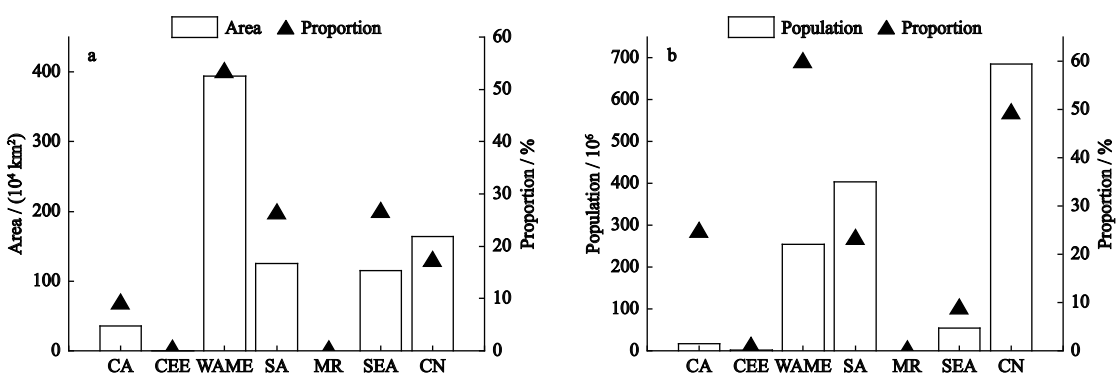

Fig. 8 Area (a) and population (b) of high suitable areas in each region along the Belt and Road (CA refers to Central Asia, CEE refers to Central and Eastern Europe, WAME refers to West Asia and the Middle East, SA refers to South Asia, MR refers to Mongolia and Russia, SEA refers to Southeast Asia, and CN refers to China)

(2) MSAs

MSAs encompass a land area of 626.19 × 10^4 km^2, accounting for 12.5% of the total area. The corresponding population is 1501.82 × 10^6, accounting for about one-third of the overall total. These people mainly live in China, CA, WAME, SA, and SEA (Fig. 7).

Compared with the other regions, SA encompasses the largest proportion of MSAs (Fig. 9), 197.59 × 10^4 km^2, or 41.41% of this total area. This region contains 907.92 × 10^6 people, more than half of the total population of SA, in excess of three-fifths of the MSA population along the B & R. MSAs in SA are mainly distributed on the Malwa and Deccan plateaus, on the eastern Ganges Plain and in southern Sri Lanka. MSAs across WAME are slightly smaller than in SA, accounting for 22.19% of total area across this region, about one-fifth of the total area of the MSA containing about one-quarter of the total population. These areas are mainly concentrated in the southeast of Egypt as well as in the north, west, and south of the Rub Khali Desert on the Arabian Peninsula. MSAs encompass 106.05 × 10^4 km^2 of China (11.05% of the total country) and contain a population of 398.74 × 10^6, in excess of one-quarter of the whole country. They are primarily located on the North China Plain, in the northeast of the Tarim Basin, across most of the Turpan Basin, in the northeast of the Yunnan-Guizhou Plateau, in the Fenwei Valley, and within mountainous and hilly areas around the Sichuan Basin. In excess of 40% of the CA population live in MSAs covering an area of 48.88 × 10^4 km^2. MSAs in both CEE and MR encompass less than 5.00 × 10^4 km^2, with a population of 6.33 × 10^6 and 2.69 × 10^6, respectively, scattered in southern coastal areas.

(3) LSAs

Data show that LSAs along the B & R encompass 1046.70 × 10^4 km^2 (20.89% of total area), including a population of 1,101.31 × 10^6 (24.05% of the total). LSAs are widely distributed across all seven regions (Fig. 7).

LSAs within China are the largest of all regions (Fig. 10); these zones are also the largest climate suitability type within this country, up to 277.88 × 10^4 km^2, close to 30% of total area and carrying 17.34% of total population. LSAs in China are mainly distributed on the Shandong Peninsula, the Northeast Plain, the Liaodong Peninsula, the southwest of the Inner Mongolia Plateau, the Loess Plateau, and the Northwest Basin. LSAs in CA, CEE, WAME, and SEA all cover an area of about 150.00 × 10^4 km^2. LSAs within SEA encompass the largest population (212.18 × 10^6), followed by CEE (159.25 × 10^6), and then less than 65.00 × 10^6 in CA and WAME. LSAs in SA and MR both encompass about 93.00 × 10^4 km^2, even though the populations of these two regions are quite different, 295.21 × 10^6 and 34.42 × 10^6, respectively. LSAs in SA are located in central Afghanistan, along the southern part of the border between Pakistan and India, and at the junction of plains and mountains in the central-eastern Indian Peninsula. LSAs in MR are mainly distributed on plains located to the north of the Greater Caucasus Mountains and to the south of the Don River.

(4) CSAs

CSAs within the B & R cover an area of 975.86 × 10^4 km^2 (19.48% of the entire region), containing a population of 411.25 × 10^6 (8.98% of the total). CSAs comprise transitional zones between suitable and unsuitable

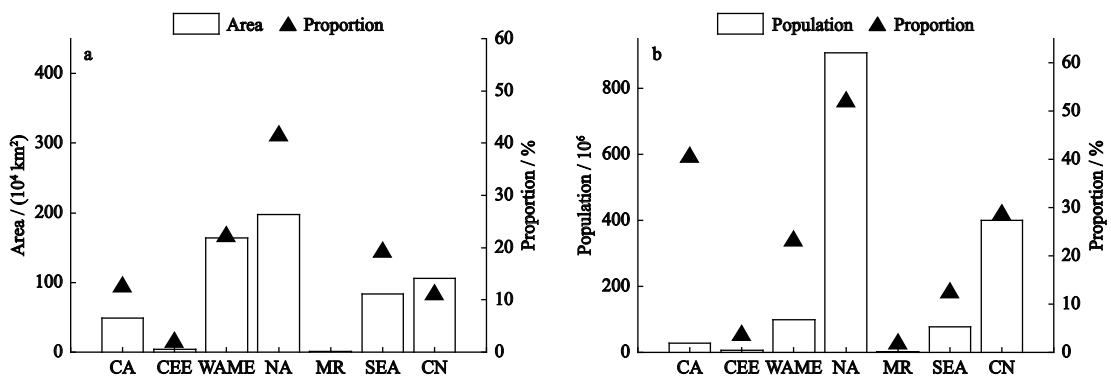

Fig. 9 Area (a) and population (b) of moderately high suitable areas in each region along the Belt and Road (CA refers to Central Asia, CEE refers to Central and Eastern Europe, WAME refers to West Asia and the Middle East, SA refers to South Asia, MR refers to Mongolia and Russia, SEA refers to Southeast Asia, and CN refers to China)

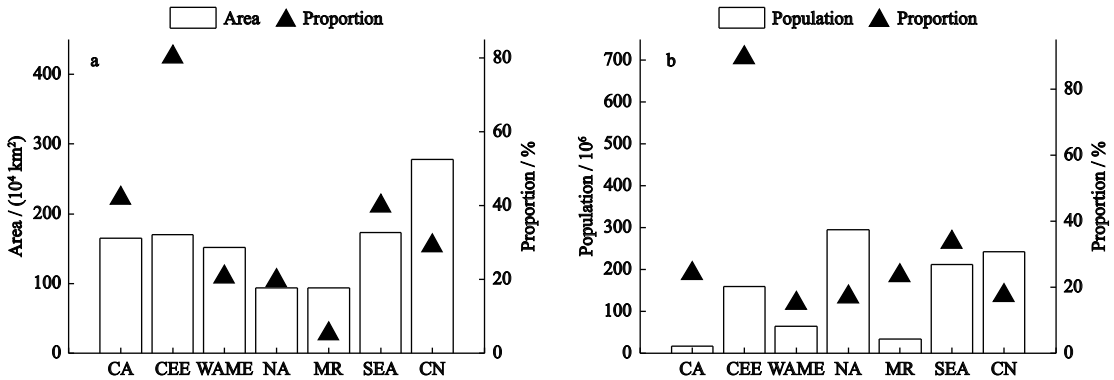

Fig. 10 Area (a) and population (b) of low suitable areas in each region along the Belt and Road (CA refers to Central Asia, CEE refers to Central and Eastern Europe, WAME refers to West Asia and the Middle East, SA refers to South Asia, MR refers to Mongolia and Russia, SEA refers to Southeast Asia, and CN refers to China)

areas along the B & R and are distributed spatially in central and northern regions (Fig. 7). The northern cold area remains sparsely populated, while the central hot area is relatively dense with people.

CSAs across MR encompass more area than other regions (Fig. 11), up to 530.11 × 10^4 km^2 (29.57% of the total MR area), in excess of half of total CSAs along the B & R. More than 70% of the total MR population live in CSAs, widely distributed on the plains of southwestern Russia as well as on the central and eastern Mongolian Plateau. CSAs in China are second most abundant to those in MR, mainly distributed in southern hinterlands and eastern mountain areas of the Qinghai-Tibet Plateau, in the surrounding mountains of the Qaidam Basin, in the Northeast Plain, and in surrounding areas within the Tianshan Mountains. CSAs in China encompass more than one-quarter of total area within this country and 4.81% of total population. Indeed, CSAs within CA account for 32.39% of the total area but only contain 10.98% of the total population, concentrated in northern Kazakhstan and the area around the Tianshan Mountains. CASs within SEA encompass an area of 63.01 × 10^4 km^2 (14.52% of total area) and contain a population of 289.06 × 10^6, the highest amongst all regions. These CASs are mainly distributed within the Chao Phraya River Basin in Thailand, the plain of Central Cambodia, the Mekong Delta in southern Vietnam, the central Philippines, and some places in Malaysia and on the Indonesian archipelago. CSAs in CEE, WAME, and SA are all less than 45.00 × 10^4 km^2; populations of CEE and WAME are about 10.00 × 10^6, while those in SA are up to 140.89 × 10^6, mainly distributed in central and eastern Afghanistan as well as within the narrow and long area at the southern foot of the Himalayas, in the southeastern coastal area of the Indian Peninsula, and in the northern coastal area of Sri Lanka. Although southern SEA and southeastern SA are CSAs, the population density is high. This is mainly because these re-

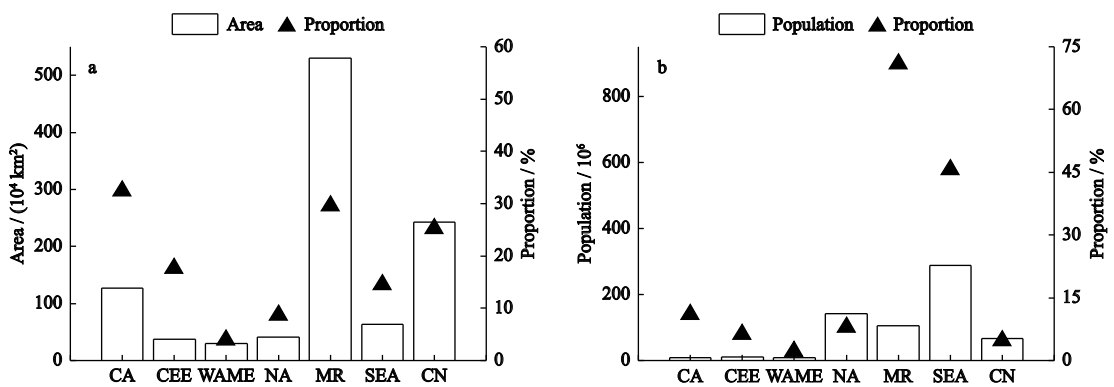

Fig. 11 Area (a) and population (b) of critically suitable areas in each region along the Belt and Road (CA refers to Central Asia, CEE refers to Central and Eastern Europe, WAME refers to West Asia and the Middle East, SA refers to South Asia, MR refers to Mongolia and Russia, SEA refers to Southeast Asia, and CN refers to China)

gions are in plain areas, with flat terrain and dense water networks which are conducive to people's production and life.

(5) NSAs

These areas within the B & R cover an area of 1,498.10 × 10^4 km^2 (29.90% of the total) and contain a population of 8.43 × 10^6 (0.18% of the total). Indeed, compared with other suitability zones, NSAs cover the largest land area but also contain the smallest population. These NSAs are highly concentrated in high-latitude and altitude areas (Fig. 7).

Around 78% of total NSAs within the B & R are in MR (Fig. 12), a significantly bigger area than other regions, concentrated in mountainous areas of northwest Mongolia, the Western Siberian Plain, the Central Siberian Plateau, and the Russian Far East. It is clear that about 65.28% of total population within NSAs along the B & R are found in this region. NSAs in China encompass an area of 169.63 × 10^4 km^2, in second place to MR, and are home to a population of 1.30 × 10^6, less than one thousandth of the total population in this country. High-latitude and altitude areas in China are NSAs, including the northern Tibet Plateau, the Qilian Mountains, the Pamirs and Tianshan Mountains, as well as the Daxingan Mountains. NSAs within CA and SA comprise both less than 20.00 × 10^4 km^2 and are concentrated in the Pamirs, the Alatau, Tianshan, and Hindu Kush mountains as well as within the narrow strip of land in the southern Himalayan foothills. NSAs in CEE and WAME encompass both less than 0.80 × 10^4 km^2 where there is very little population. Climate within the SEA is relatively good and no NSAs are present.

4 Discussion

The climate suitability assessment of the human settlements can reveal the matching degree of population distribution and climatic conditions. The assessment results can help guide the reasonable distribution of population and provide a scientific basis for the territorial and spatial planning of various countries and regions. In this study, the previous climate suitability zoning standards (Tang et al., 2008; Zhong et al., 2019) were revised based on the correlation between THI and population distribution, and a new set of climate suitability zoning standards suitable for the B & R were obtained. The climate suitability assessment along the B & R in this study was carried out given the premise that people do not rely on any equipment and facilities to cope with either a cold or hot climate. Though this approach does not take into account the contribution of science and technology to population resistance to adverse climatic conditions, the results of this study show a high degree of spatial consistency between population distribution and climate suitability zoning. In addition, our results are similar to those obtained by Tang et al. (2008) and Kong (2020): in general, the climate suitability is generally distributed in a zonal pattern, decreasing from low altitude areas to high altitude areas on the same latitude (except SA and SEA), and decreasing from the southeast to the northwest in China. The above results show that the assessment method used in this study can reasonably reveal the spatial distribution of the climate suitability for the B & R.

The countries and regions along the B & R are vast, with large north-south spans, different terrains, diverse

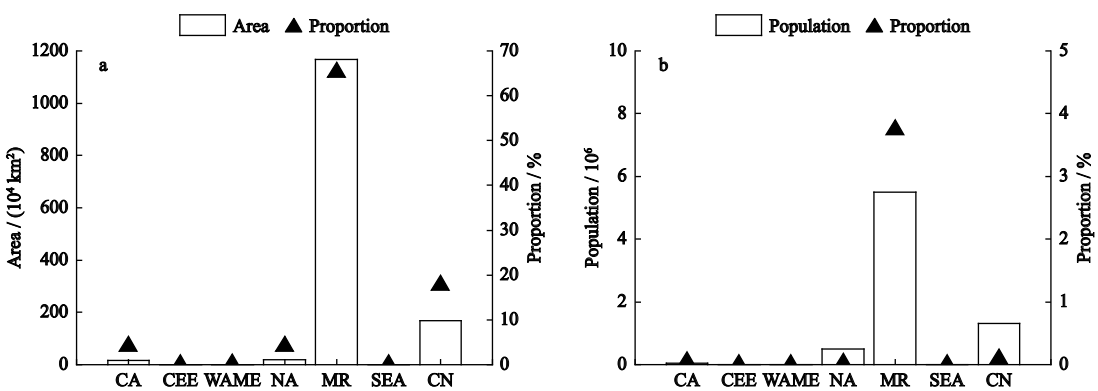

Fig. 12 Area (a) and population (b) of non-suitable areas in each region along the Belt and Road (CA refers to Central Asia, CEE refers to Central and Eastern Europe, WAME refers to West Asia and the Middle East, SA refers to South Asia, MR refers to Mongolia and Russia, SEA refers to Southeast Asia, and CN refers to China)

mountain ranges, and complex climate. Using a single standard to evaluate the climate suitability of this vast area could weaken the differences in people's adaptability to the local climate in different regions. Therefore, it remains a key scientific issue that needs to be deeply discussed to quantitatively delimit the range of biometeorological indices (such as THI) for different climate suitability areas according to the human acclimatization of different regions. In addition, the climate suitability evaluation of this study is mainly based on the multi-year average temperature and relative humidity data. In fact, the factors that affect climate suitability include precipitation, solar radiation, air pressure, vegetation coverage and so on (Kong et al., 2019). Therefore, in the future research, it is necessary to fully explore the impacts of multiple factors in consideration of the availability of data, in order to conduct a comprehensive and objective evaluation of the climate suitability of the human settlements.

The continuous warming and the high frequency of extreme weather events under climate change will cause the climate suitability of each region to change. However, fine-grained projection of climate suitability is scarce. Therefore, time dynamic evaluations or predictions of climatic suitability based on the technology-driven application of big data and future climate scenarios (Kubo et al., 2020; Liu et al., 2020) is expected to launch in the future, which can enrich our understanding of climate change impacts on human settlements.

5 Conclusions

The THI was calculated based on the multi-year mean temperature and relative humidity at a 1 km spatial resolution for the B & R. The correlation results between population distribution and this index was the basis for the determination of the climate suitability zoning criteria which enabled us to evaluate the climate suitability of human settlements for the B & R. The following conclusions were drawn from the results of the analysis:

(1) THI values for areas along the B & R have experienced a significant fluctuating downward trend from south to north as latitude increases. Values for THI in most regions are between 35 and 75. The area of extremely cold regions with THI value less than 35 accounts for nearly 30% of the entire region. These regions are mainly located in high-latitude and altitude regions. Regions with THI values greater than 75 tend to have muggy climates.

(2) The population distribution of areas along the B & R is significantly correlated with the THI when THI values are higher than 35. Thus, the correlation between population distribution and THI can be used as a basis for determining climate suitability zoning criteria. This method provides a new perspective and reference for determining the suitability assessment criteria of human settlements.

(3) The results of climate suitability zones show that regions with suitable climate including HSAs, MSAs, and LSAs account for 50.62% of total area and contain in excess of 90% of the total population. These areas are widely distributed in the southern region of 45°N latitude with the exception of the Qinghai-Tibet Plateau. HSAs are mainly distributed within the southeastern part of China, within the northern part of the Southeastern Peninsula, and across most parts of WAME. CSAs encompass 19.48% of the entire area and contain 8.98% of the total population; these are mainly distributed in the southwestern MR, in the southern and eastern parts of the Qinghai-Tibet Plateau, in eastern parts of the Northeast Plain, in northern CA, in northern CEE, in parts of WAME, in southeast coastal areas of SA, and across the southern Indochina Peninsula. NSAs account for less than 30% of total area; these are concentrated in the MR, on the Chinese Qinghai-Tibet Plateau, and in other cold high-latitude and altitude areas. These regions encompass just 0.18% of the total population.

References

Adiguzel F, Cetin M, Kaya E et al., 2020. Defining suitable areas for bioclimatic comfort for landscape planning and landscape management in Hatay, Turkey. *Theoretical and Applied Climatology*, 139(3): 1493–1503. doi: 10.1007/s00704-019-03065-7

Aghamohammadi N, Fong CS, Idrus MHM et al., 2021. Environmental heat-related health symptoms among community in a tropical city. *Science of the Total Environment*, 782: 146611. doi: 10.1016/j.scitotenv.2021.146611

Amininia K, Abad B, Safarianzengir V et al., 2020. Investigation and analysis of climate comfort on people health tourism in Ardabil province, Iran. *Air Quality, Atmosphere & Health*, 13(1): 1293–303. doi: 10.1007/s11869-020-00883-x

Błażejczyk A, Błażejczyk K, Baranowski J et al., 2018. Heat stress mortality and desired adaptation responses of healthcare system in Poland. *International Journal of Biometeorology*, 62(3): 307–318. doi: 10.1007/s00484-017-1423-0

Cheng Q P, Zhong F L, 2019. Evaluation of tourism climate comfort in the Grand Shangri-La region. *Journal of Mountain Science*, 16(6): 1452–1469. doi: 10.1007/s11629-018-5081-4

Di Napoli C, Pappenberger F, Cloke H L, 2018. Assessing heat-related health risk in Europe via the Universal Thermal Climate Index (UTCI). *International Journal of Biometeorology*, 62(7): 1155–1165. doi: 10.1007/s00484-018-1518-2

Dong T Y, Dong W J, Guo Y et al., 2018. Future temperature changes over the critical Belt and Road region based on CMIP5 models. *Advances in Climate Change Research*, 9(1): 57–65. doi: 10.1016/j.accre.2018.01.003

Emmanuel R, 2005. Thermal comfort implications of urbanization in a warm-humid city: the Colombo Metropolitan Region (CMR), Sri Lanka. *Building and Environment*, 40(12): 1591–1601. doi: 10.1016/j.buildenv.2004.12.004

Han T T, Chen H P, Hao X et al., 2018. Projected changes in temperature and precipitation extremes over the Silk Road Economic Belt regions by the Coupled Model Intercomparison Project Phase 5 multi-model ensembles. *International Journal of Climatology*, 38(11): 4077–4091. doi: 10.1002/joc.5553

Hartgill T W, Bergersen T K, Pirhonen J, 2011. Core body temperature and the thermoneutral zone: a longitudinal study of normal human pregnancy. *Acta Physiologica*, 201(4): 467–474. doi: 10.1111/j.1748-1716.2010.02228.x

Hsiang S M, Burke M, Miguel E, 2013. Quantifying the influence of climate on human conflict. *Science*, 341(6151): 1235367. doi: 10.1126/science.1235367

Huang Y P, 2016. Understanding China's Belt & Road Initiative: Motivation, framework and assessment. *China Economic Review*, 40: 314–321. doi: 10.1016/j.chieco.2016.07.007

Karger D N, Conrad O, Böhner J et al., 2017. Climatologies at high resolution for the Earth land surface areas. *Scientific Data*, 4: 170112. doi: doi: 10.1038/sdata.2017.122

Kariminia S, Motamedi S, Shamshirband S et al., 2016. Adaptation of ANFIS model to assess thermal comfort of an urban square in moderate and dry climate. *Stochastic Environmental Research & Risk Assessment*, 30(4): 1189–1203. doi: 10.1007/s00477-015-1116-3

Kjellstrom T, Briggs D, Freyberg C et al., 2016. Heat, human performance, and occupational health: a key issue for the assessment of global climate change impacts. *Annual Review of Public Health*, 37: 97–112. doi: 10.1146/annurev-publhealth-032315-021740

Kong Q Q, Zheng J Y, Fowler H J et al., 2019. Climate change and summer thermal comfort in China. *Theoretical and Applied Climatology, 137*, 1077–1088. doi: 10.1007/s00704-018-2648-5

Kong Feng, 2020. Multi-temporal scale assessment of climate comfort of habitat environment and spatial differences in China. *Journal of Arid Land Resources and Environment*, 34(3): 102–111. (in Chinese)

Kubo T, Uryu S, Yamano H et al., 2020. Mobile phone network data reveal nationwide economic value of coastal tourism under climate change. *Tourism Management*, 77: 104010. doi: 10.1016/j.tourman.2019.104010

Liu J, Yang L Y, Zhou H Yet al., 2020. Impact of climate change on hiking: quantitative evidence through big data mining, *Current Issues in Tourism*. doi: 10.1080/13683500.2020.1858037

Matthews T K R, Wilby R L, Murphy C, 2017. Communicating the deadly consequences of global warming for human heat stress. *Proceedings of the National Academy of Sciences of the United States of America*, 114(15): 3861–3866. doi: 10.1073/pnas.1617526114

Mayer H, Höppe P, 1987. Thermal comfort of man in different urban environments. *Theoretical and Applied Climatology*, 38(1): 43–49. doi: 10.1007/BF00866252

Mora C, Dousset B, Caldwell I R, et al., 2017. Global risk of deadly heat. *Nature Climate Change*, 7(7): 501−506. **7**, 501−6. doi: 10.1038/nclimate3322

Müller N, Kuttler W, Barlag A B, 2014. Counteracting urban climate change: adaptation measures and their effect on thermal comfort. *Theoretical & Applied Climatology*, 115(1−2): 243–257. doi: 10.1007/s00704-013-0890-4

Nalau J, Becken S, Noakes S et al., 2017. Mapping tourism stakeholders 'weather and climate information seeking behavior in Fiji. *Weather Climate and Society*, 9(3): 377–391. doi: 10.1175/WCAS-D-16-0078.1

Oleson K W, Monaghan A, Wilhelmi O et al., 2015. Interactions between urbanization, heat stress, and climate change. *Climatic Change*, 129(3−4): 525–541. doi: 10.1007/s10584-013-0936-8

Oliver J E, 1973. Climate and man's environment: an introduction to applied climatology. *New York: John Wiley & Sons, Inc.*

Pallubinsky H, Schellen L, Kingma B R M et al., 2015. Human thermoneutral zone and thermal comfort zone: effects of mild heat acclimation. *Extreme Physiology & Medicine*, 4(Suppl 1): A7. doi: 10.1186/2046-7648-4-S1-A7

Pallubinsky H, Schellen L, Van Marken Lichtenbelt W D, 2019. Exploring the human thermoneutral zone— a dynamic approach. *Journal of Thermal Biology*, 79: 199–208. doi: 10.1016/j.jtherbio.2018.12.014

Rupp R F, Vásquez N G, Lamberts R, 2015. Areview of human thermal comfort in the built environment.. *Energy & Buildings*, 105: 178–205. doi: 10.1016/j.enbuild.2015.07.047

Tang C C, Zhong L S, Kristen M et al., 2012. A comprehensive evaluation of tourism climate suitability in Qinghai Province, China. *Journal of Mountain Science*, 9(3): 403–413. doi: 10.1007/s11629-009-2161-5

Tang Yan, Feng Zhiming, Yang Yanzhao, 2008. Evaluation of climate suitability for human settlement in China. *Resources Science*, 30(5): 648–653. (in Chinese)

Terjung W H, 1966. Physiologic climates of the conterminous United States: a bioclimatic classification based on man. *Annals of the Association of American Geographers*, 56(1): 141–179. doi: 10.1111/j.1467-8306.1966.tb00549.x

Toy S, Kántor N, 2017. Evaluation of human thermal comfort ranges in urban climate of winter cities on the example of Erzurum city. *Environmental Science and Pollution Research*,

24(2): 1811–1820. doi: 10.1007/s11356-016-7902-8

Vaneckova P, Neville G, Tippett V et al., 2011. Do biometeorological indices improve modeling outcomes of heat-related mortality? *Journal of Applied Meteorology and Climatology*, 50(6): 1165–1176. doi: 10.1175/2011JAMC2632.1

Vezzulli L, Grande C, Reid P C et al., 2016. Climate influence on Vibrio and associated human diseases during the past half-century in the coastal North Atlantic. *Proceedings of the National Academy of Sciences of the United States of America*, 113(34): E5062–E5071. doi: 10.1073/pnas.1609157113

Word Bank, 2020. *World Bank Open Data*. Available at https://data.worldbank.org.cn/.

Wu X X, Lu Y M, Zhou S et al., 2016. Impact of climate change on human infectious diseases: empirical evidence and human adaptation. *Environment International*, 86: 14–23. doi: 10.1016/j.envint.2015.09.007

Xu F, 2018. *Belt and Road: Culture and Communications Aiming at Great Unity*. In: The Belt and Road. Singapore: Springer, 49−74. doi: 10.1007/978-981-13-1105-5_3

Yang W, Wong N H, Li C Q, 2016. Effect of street design on outdoor thermal comfort in an urban street in Singapore. *Journal of Urban Planning & Development*, 142(1): 05015003. doi: 10.1061/(ASCE)UP.1943-5444.0000285

You Zhen, Feng Zhiming, Yang Yanzhao et al., 2020. Evaluation of human settlement environmental suitability in Tibet based on gridded data. *Resources Science*, 42(2): 394–406. (in Chinese)

Zhao J Y, Wang S J, 2021. Spatio-temporal evolution and prediction of tourism comprehensive climate comfort in Henan Province, China. *Atmosphere*.12(7): 823. doi: 10.3390/atmos12070823 (Published online)

Zhong L S, Yu H, Zeng Y X, 2019. Impact of climate change on Tibet tourism based on tourism climate index. *Journal of Geographical Sciences*, 29(12): 2085–2100. doi: 10.1007/s11442-019-1706-y